

Received April 9, 2020, accepted May 3, 2020, date of publication May 14, 2020, date of current version June 4, 2020.

Digital Object Identifier 10.1109/ACCESS.2020.2994550

# Fast Radix-32 Approximate DFTs for 1024-Beam Digital RF Beamforming

ARJUNA MADANAYAKE<sup>1</sup>, (Member, IEEE), RENATO J. CINTRA<sup>2,7</sup>, (Senior Member, IEEE),  
NAJATH AKRAM<sup>1</sup>, (Student Member, IEEE),  
VIDUNETH ARIYARATHNA<sup>1</sup>, (Student Member, IEEE),  
SOUMYAJIT MANDAL<sup>3</sup>, (Senior Member, IEEE), VÍTOR A. COUTINHO<sup>4</sup>, FÁBIO M. BAYER<sup>5</sup>,  
DIEGO COELHO<sup>2</sup>, AND THEODORE S. RAPPAPORT<sup>6</sup>, (Fellow, IEEE)

<sup>1</sup>Electrical and Computer Engineering Department, Florida International University, Miami, FL 33199, USA

<sup>2</sup>Signal Processing Group, Departamento de Estatística, UFPE, 50670-901 Recife, Brazil

<sup>3</sup>Electrical, Computer, and Systems Engineering Department, Case Western Reserve University, Cleveland, OH 44106, USA

<sup>4</sup>Signal Processing Group, Departamento de Estatística, UFPE, 50670-901 Recife, Brazil

<sup>5</sup>Department of Statistics and LACESM, Federal University of Santa Maria, 97105-900 Santa Maria, Brazil

<sup>6</sup>NYU Wireless, Department of Electrical Engineering, Tandon School of Engineering, New York University, Brooklyn NY 11220, USA

<sup>7</sup>Department of Electrical and Computer Engineering, University of Calgary, Calgary, AB T2N 1N4, Canada

Corresponding author: Arjuna Madanayake (amadanay@fiu.edu)

This work was supported in part by multiple awards from NSF Collaborative Research: Spatially Oversampled Dense Multi-Beam Millimeter-Wave Communications for Exponentially Increased Energy-Efficiency (SpecEES) under Award 1854798 and Award 1731290, in part by NSF ECCS, in part by Collaborative Research: Wideband Multi-Beam Antenna Arrays: Low-Complexity Algorithms and Analog-CMOS Implementations under Award 1711395, and in part by Conselho Nacional de Desenvolvimento Científico e Tecnológico (CNPq), Brazil.

**ABSTRACT** The discrete Fourier transform (DFT) is widely employed for multi-beam digital beamforming. The DFT can be efficiently implemented through the use of fast Fourier transform (FFT) algorithms, thus reducing chip area, power consumption, processing time, and consumption of other hardware resources. This paper proposes three new hybrid DFT 1024-point DFT approximations and their respective fast algorithms. These approximate DFT (ADFT) algorithms have significantly reduced circuit complexity and power consumption compared to traditional FFT approaches while trading off a subtle loss in computational precision which is acceptable for digital beamforming applications in RF antenna implementations. ADFT algorithms have not been introduced for beamforming beyond  $N = 32$ , but this paper anticipates the need for massively large adaptive arrays for future 5G and 6G systems. Digital CMOS circuit designs for the ADFTs show the resulting improvements in both circuit complexity and power consumption metrics. Simulation results show similar or lower critical path delay with up to 48.5% lower chip area compared to a standard Cooley-Tukey FFT. The time-area and dynamic power metrics are reduced up to 66.0%. The 1024-point ADFT beamformers produce signal-to-noise ratio (SNR) gains between 29.2–30.1 dB, which is a loss of  $\leq 0.9$  dB SNR gain compared to exact 1024-point DFT beamformers (worst case) realizable at using an FFT.

**INDEX TERMS** Fourier transform, discrete fourier transform, approximation, VLSI, DFT, FFT, radix, fast algorithm, beamforming, beamsteering, 5G, MIMO, massive MIMO.

## I. INTRODUCTION

The discrete Fourier transform (DFT) is a linear transform that is widely applied to convert a sampled signal into a representation over the discrete frequency domain. Fully-digital transmit and receive aperture arrays for radio-frequency (RF) spectrum sensing, communications, and radar use the DFT

The associate editor coordinating the review of this manuscript and approving it for publication was Pietro Savazzi<sup>1</sup>.

for multi-beam beamforming. For example, simultaneous receiver beams are imperative for high-capacity multi-input multi-output (MIMO) wireless communication systems. Joint spatial division and multiplexing (JSDM) is an approach to multi-user MIMO downlinks that exploits the structure of channel correlations in order to allow a large number of antennas at the base station while requiring reduced-dimensional channel state information at the transmitter [1], [2]. This uses a multi-user MIMO downlink precoder obtained from

an array pre-beamforming matrix, and incurs no loss of optimality for a large number of array elements. A DFT-based pre-beamforming matrix is near-optimal for uniform linear arrays (ULAs) of antennas, and requires only coarse information about the users' angles of arrival and angular spread [3].

The  $N$ -point DFT computes  $N$  uniformly spaced frequency domain outputs ("bins") using  $N$  uniformly sampled discrete signal values by means of an  $N \times N$  transform matrix [4]. Because implementations of the multiplication operation requires more chip area (or processing time, for non-parallelized software implementations) compared to addition operations, the computational complexity of computing the DFT is expressed in terms of the multiplication count [5]. The required number of multiplications depends on the fast algorithm employed for the particular transform length  $N$  in consideration. The computational complexity of the  $N$ -point DFT using direct matrix-vector multiplication is  $\mathcal{O}(N^2)$  where  $\mathcal{O}(\cdot)$  represents the "big O" notation for asymptotic complexity [6]–[8].

The computational complexity of computing the  $N$ -point DFT can be reduced via fast Fourier transforms (FFTs), which are fast algorithms for realizing DFTs that reduce the computational complexity to  $\mathcal{O}(N \log_2 N)$  [5]. Thus, multiple DFT beams for both wireless communications applications (e.g., JSDM) and multi-beam radar/imaging systems are often generated by applying an  $N$ -point spatial FFT to each temporal sample acquired by the ULA [9], [10].

The search for particular  $N$ -point FFT methods that minimize the multiplicative complexity is a separate field of research in signal processing, computer science, and applied mathematics, with a multitude of algorithms and implementations available [5], [11]–[14]. In [15], the theoretical lower bound for the DFT multiplicative complexity was established as a function of  $N$ . All FFT algorithms use sparse factorizations of the DFT matrix to provide accurate implementations of the DFT at an arithmetic complexity that approaches this lower bound. However, such high accuracy is of limited practical relevance in digital multi-beam RF beamforming applications, such as radar signal processing, where the accuracy of the results is limited by other system parameters or environmental conditions (e.g., thermal noise in a receiver, or the practical implementation of an antenna radiation pattern compared to ideal, harmonic distortion in a microwave mixer or amplifier). In such applications, relentless pursuit of high accuracy in the exact computation of the DFT is not relevant in terms of overall performance, and smart system designers can exploit this fact for power and cost optimization. High-precision VLSI implementation of FFT algorithms may result in unnecessarily large circuits, exaggerated critical path delays, and wasted power. All of those factors contribute to higher-cost circuits, reduced frequency of operation, and higher operation costs. This is because digital multipliers demand a large amount of circuit resources when compared to simple adders. This makes the reduction of the number of multipliers in a given system crucial when chip area and power must be conserved and

high-speed operation is desirable. In particular, the adoption of approximate DFT (ADFT) computations opens up new possibilities for fast algorithms which do not compute the DFT in the strictest mathematical sense, but nevertheless can be *good enough* for digital multi-beam RF beamforming applications, particularly at mmwave frequencies and above, where reproducibility of antenna patterns become more problematic. Because ADFT applications are able to realize much greater efficiencies than the theoretical lower bound  $N$  for an  $N$ -point DFT proposed in [15], ADFT computations allow greater reductions in computational complexity than traditional FFTs, albeit at the cost of a deterministic loss in performance, namely a small increase in worst-case side-lobe level [16].

The ever increasing data rate demands of wireless communications led to the exploration of millimeter-wave (mmW)/sub-THz/THz frequencies in 5G cellular networks [17], [18], where larger antenna array sizes (e.g.  $N = 64, 128, 256$ ) for beamforming and massive MIMO have become a general requirement [19]. For example, IoT and robotics applications in emerging fifth-generation (5G) and beyond mobile wireless networks will require 6D positioning, which involves both spatial position and device orientation (role, pitch, yaw) which require new algorithms that can benefit from large number of closely packed low-complexity digital beams [2], [20], [21]. A similar need occurs in the design of systems for intelligent surfaces which provide means of communication without line-of-sight [22]. In fact mmW-based 5G MIMO cellular systems are already being deployed [23]. Moreover, ongoing research in the sub-THz range [2], [24]–[32] suggests that the W and G bands will be commercially available within the next 5-10 years. Such sub-THz carrier frequencies require large amounts of beamforming gain to mitigate free-space path loss in the first meter of propagation from the antenna [2], [18], [33], [34]. Thus, communication systems at these frequencies would require much larger numbers of antenna elements in the transceiver arrays; array sizes of the order of  $N = 1000$  elements would not be unrealistic for future sixth generation (6G) cellular systems. Nevertheless, to the best of our knowledge, DFT approximations in the literature are limited to  $N \leq 32$ .

In this paper, we address this important beamforming challenge by introducing three new approximations to the very large  $N = 1024$  (1024-point) DFT. Fast algorithms that allow low-complexity implementations of these approximations are also developed and shown to provide remarkable accuracy with significant cost and power reduction compared to DFT and FFT approaches. The proposed 1024-point ADFTs are based on a recently proposed 32-point DFT approximation and multiplierless fast algorithm [7], [35] that furnish a "reasonable" approximation of the 32-point DFT albeit without using multiplications (i.e., using an adder-only signal flow graph). The 1024-point exact DFT can be expressed in terms of 32-point DFT. We use this fact to derive an approximation for the 1024-point DFT matrix by means for our earlier 32-point ADFT. In particular, we propose three different

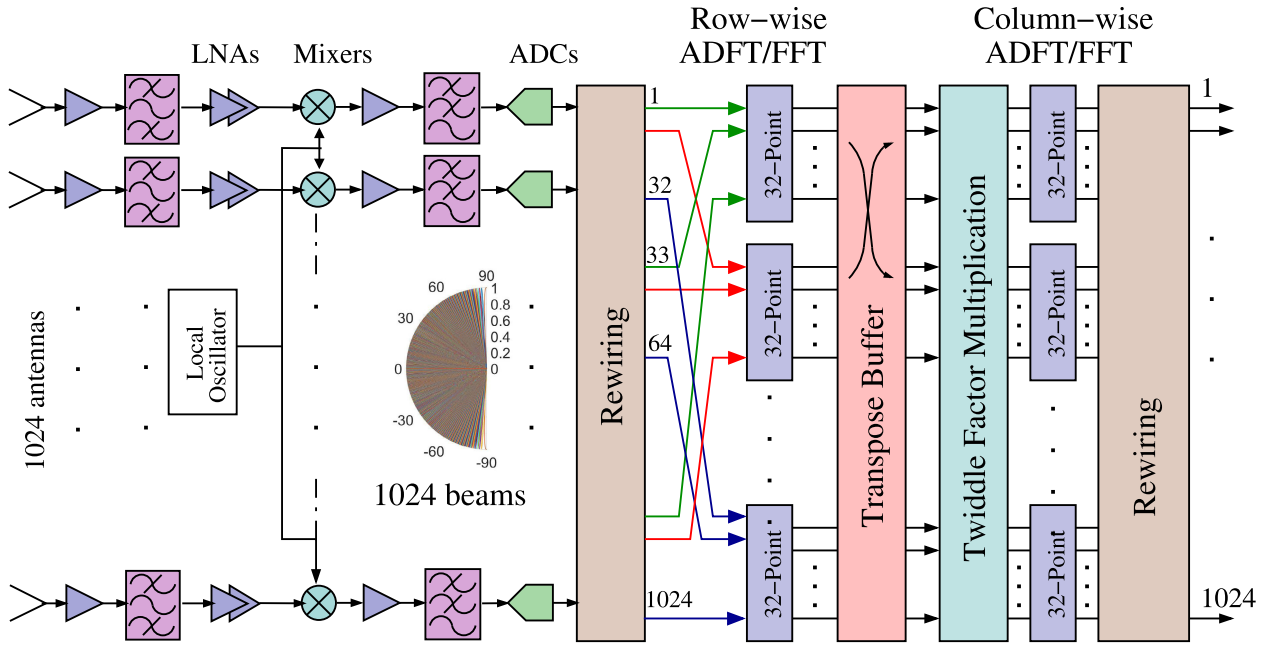


**FIGURE 1.** Beamforming architecture of a 1024-element ULA receiver using the proposed method. The rewiring block performs spatial multiplexing over the incoming in the input and the transformed signal at the output (see Fig. 5).

1024-point transforms with different trade-offs in computational complexity and computational accuracy compared to the baseline exact DFT. These three transforms differ from each other based on the use of 32-point ADFT in the derivation and they can be used to replace the FFT while generating  $N = 1024$  beams from a 1024-element ULA as shown in Fig. 1.

The paper is organized as follows. Section II reviews the DFT and selected popular FFT algorithms. In Section III, we discuss the mathematical background for the 32-point DFT approximation introduced in [35] and describe its associated fast algorithm in matrix form. In Section IV, we present 1024-point DFT approximations and discuss three different algorithms to implement them. Section V explores the digital VLSI realization of the proposed 1024-point DFT approximations. In Section VI, we summarize our conclusions.

## II. REVIEW OF THE DFT AND FFT

In order to understand the method used to create accurate ADFT algorithms, we will discuss the mathematical background related to the DFT definition and FFT algorithms.

### A. MATHEMATICAL DEFINITION OF THE DFT

Let the vector  $\mathbf{x} = [x[0] \ x[1] \ \dots \ x[N-1]]^T$  represent a signal with  $N$  samples. The DFT maps the input signal  $\mathbf{x}$  into an output signal  $\mathbf{X} = [X[0] \ X[1] \ \dots \ X[N-1]]^T$  according to the following relationship:

$$X[k] \triangleq \frac{1}{\sqrt{N}} \sum_{n=0}^{N-1} x[n] \cdot \omega_N^{nk}, \quad k = 0, 1, \dots, N-1, \quad (1)$$

where  $\omega_N = e^{-j\frac{2\pi}{N}}$  is the  $N$ th root of unity and  $j \triangleq \sqrt{-1}$ . On the other hand, the inverse DFT (IDFT) is given as

$$x[n] = \frac{1}{\sqrt{N}} \sum_{k=0}^{N-1} X[k] \cdot \omega_N^{-nk}, \quad n = 0, 1, \dots, N-1. \quad (2)$$

The DFT of  $\mathbf{x}$  can be expressed through a matrix-vector multiplication  $\mathbf{X} = \mathbf{F}_N \cdot \mathbf{x}$ , where

$$\mathbf{F}_N = \frac{1}{\sqrt{N}} \begin{bmatrix} 1 & 1 & 1 & \dots & 1 \\ 1 & \omega_N & \omega_N^2 & \dots & \omega_N^{(N-1)} \\ 1 & \omega_N^2 & \omega_N^4 & \dots & \omega_N^{2(N-1)} \\ 1 & \omega_N^3 & \omega_N^6 & \dots & \omega_N^{3(N-1)} \\ \vdots & \vdots & \vdots & \ddots & \vdots \\ 1 & \omega_N^{(N-1)} & \omega_N^{2(N-1)} & \dots & \omega_N^{(N-1)(N-1)} \end{bmatrix} \quad (3)$$

is the  $N$ -point DFT matrix [36].

### B. FFT ALGORITHMS

DFT was originally the cornerstone of primitive DSP, until the FFT was found to be vastly more efficient. Here we extend FFTs to become ADFTs. The computational complexity associated with performing the  $N$ -point DFT operation in direct form is  $\mathcal{O}(N^2)$ . This complexity is prohibitive for most engineering applications since a high number of operations accounts for (i) higher energy consumption; (ii) higher latency; (iii) higher number of gates; and, in consequence, (iv) higher chance of system failure. To address these issues, FFT factorizations furnish a product of sparse (mostly zeros) matrices that reduces the DFT computational complexity to  $\mathcal{O}(N \log N)$ . Different FFT algorithms can be identified in the literature [37]–[40]. Here we consider three popular algorithms, namely i) the Cooley-Tukey FFT [5], ii) the split-radix FFT [38], and iii) the Winograd FFT [41]; each of these is briefly described below.

1) COOLEY-TUKEY ALGORITHM

A very popular form of the classical Cooley-Tukey algorithm is the radix-2 decimation-in-time FFT, which splits the  $N$ -point DFT computation into two  $N/2$ -point DFT computations resulting in an overall reduced complexity [37]. Recursive use of this algorithm reduces the number of multiplications of the DFT from  $\mathcal{O}(N^2)$  down to  $\mathcal{O}(N \log_2 N)$ .

2) SPLIT-RADIX ALGORITHM

This is a variant of the Cooley-Tukey FFT algorithm which uses a blend of radix-2 and radix-4 by recursively expressing the  $N$ -point DFT in terms of one  $N/2$ -point DFT and two  $N/4$ -point DFT instantiations [38]. The split-radix algorithm can reduce the overall number of additions required to compute DFTs of sizes that are powers of two without increasing the number of multiplications [42].

3) WINOGRAD ALGORITHM

The Winograd algorithm implements an efficient FFT and exploits the multiplicative structure on the data indexing of DFT and converts it into a cyclic convolution computation [39], [40]. In several particular cases, the Winograd algorithm achieves the theoretical minimum multiplicative complexity [15] as shown in [39] making it more efficient over the Cooley-Tukey and radix. For large DFT block lengths that can be decomposed as a product of small primes, the Winograd algorithm achieves nearly-linear complexity [5].

C. MATRIX REPRESENTATION OF THE  $N^2$ -POINT DFT IN TERMS OF THE  $N$ -POINT DFT

Now we will use the matrix definition in sub section II-A to derive a matrix representation for the computation of the  $N^2$ -point DFT in terms of the  $N$ -point DFT via a radix- $N$  FFT approach. The goal of this is to derive a 1024-point DFT in terms of 32-point DFT. Generally speaking, the  $N^2$ -point DFT computation corresponds to a vector-matrix multiplication with a  $N^2 \times N^2$  matrix transformation:

$$\mathbf{X} = \mathbf{F}_{N^2} \cdot \mathbf{x}. \tag{4}$$

The expression in (4) can be rewritten by directly invoking the Cooley-Tukey algorithm in its more general form as detailed in [5, p. 69]. By explicitly following the Cooley-Tukey algorithm, the  $N^2$ -point DFT can be computed by means of:

- 1) address-shuffling the input column vector into a 2D  $N \times N$  array;
- 2) computing the  $N$ -point DFT of each array column using FFTs;
- 3) element-wise multiplying the twiddle-factors (twiddle factors are the coefficients containing roots of unity in the DFT matrix [5]);
- 4) computing the  $N$ -point DFT of each resulting row using FFTs; and
- 5) undoing the address shuffling to convert the obtained 2D array into the final output column vector.

The 1D to 2D mapping can be accomplished by means of the inverse vectorization operator  $\text{invvec}(\cdot)$  [43] (Cf. [44], [45]) which obeys the following mapping:

$$\text{invvec} \left( \begin{bmatrix} x_0 \\ x_1 \\ \vdots \\ x_{N^2} \end{bmatrix} \right) = \begin{bmatrix} x_0 & x_N & \cdots & x_{N(N-1)} \\ x_1 & x_{N+1} & \cdots & x_{N(N-1)+1} \\ \vdots & \vdots & \ddots & \vdots \\ x_{N-1} & x_{2N-1} & \cdots & x_{N^2-1} \end{bmatrix}. \tag{5}$$

Based on the 1D to 2D mapping in Eqn. (5) we can show that the  $N^2$ -point DFT given in (4) can be represented in the following matrix expression based on the Cooley-Tukey algorithm:

$$\mathbf{X} = \text{vec} \left( \left\{ \mathbf{F}_N \cdot \left[ \Omega_N \circ \left( \mathbf{F}_N \cdot (\text{invvec}(\mathbf{x}))^\top \right) \right]^\top \right\}^\top \right), \tag{6}$$

where  $\text{vec}(\cdot)$  is the matrix vectorization operator [46, p. 239],  $\circ$  is the Hadamard element-wise multiplication [46, p. 251], the superscript  $\top$  denotes simple transposition (non Hermitian), and  $\Omega_N$  is the twiddle-factor matrix given by  $\Omega_N = (\omega_{N^2}^{m \cdot n})_{m,n=0,1,\dots,N}$ . Noting that  $\Omega_N^\top = \Omega_N$ , (6) can be further simplified. In particular, for  $N = 1024 = 32^2$ , we have

$$\mathbf{X} = \text{vec} \left( \left[ \Omega_{32} \circ \left( \mathbf{F}_{32} \cdot (\text{invvec}(\mathbf{x}))^\top \right) \right] \cdot \mathbf{F}_{32}^\top \right). \tag{7}$$

The inner DFT call corresponds to row-wise transformation of  $\text{invvec}(\mathbf{x})$ , whereas the outer DFT performs column-wise transformations on the resulting intermediate computation. The formulation shown in (7) is the fundamental expression on which the proposed approximations (eg. ADFTs) in this work are based.

III. MULTIPLIERLESS 32-POINT ADFT

In this section, the adopted multiplierless 32-point ADFT, first introduced in [7], [35], is presented, and its complexity and error analysis are discussed. This is critical for understanding as the 1024-point ADFT is realized using 32-point ADFT as the main building block.

A. MATRIX REPRESENTATION

The considered 32-point ADFT matrix denoted by  $\hat{\mathbf{F}}_{32}$  can be computed through a product of sparse matrices whose real and imaginary parts of its coefficients contains only  $\pm 1$  entries. Such simple arithmetic leads to hardware designs that can be realized with adders only.

To present the factorization of  $\hat{\mathbf{F}}_{32}$ , we need the auxiliary structures in eq. (8)- (17), since the auxiliary factors are key for matrix factorization. Let  $\mathbf{B}_t$  be a  $t \times t$  real matrix given by

$$\mathbf{B}_t = \begin{cases} \begin{bmatrix} \mathbf{I}_{(t-1)/2} & \bar{\mathbf{I}}_{(t-1)/2} \\ & 1 \\ \bar{\mathbf{I}}_{(t-1)/2} & -\mathbf{I}_{(t-1)/2} \end{bmatrix}, & \text{if } t \text{ is odd,} \\ \begin{bmatrix} \mathbf{I}_{t/2} & \bar{\mathbf{I}}_{t/2} \\ \bar{\mathbf{I}}_{t/2} & -\mathbf{I}_{t/2} \end{bmatrix}, & \text{if } t \text{ is even,} \end{cases} \tag{8}$$







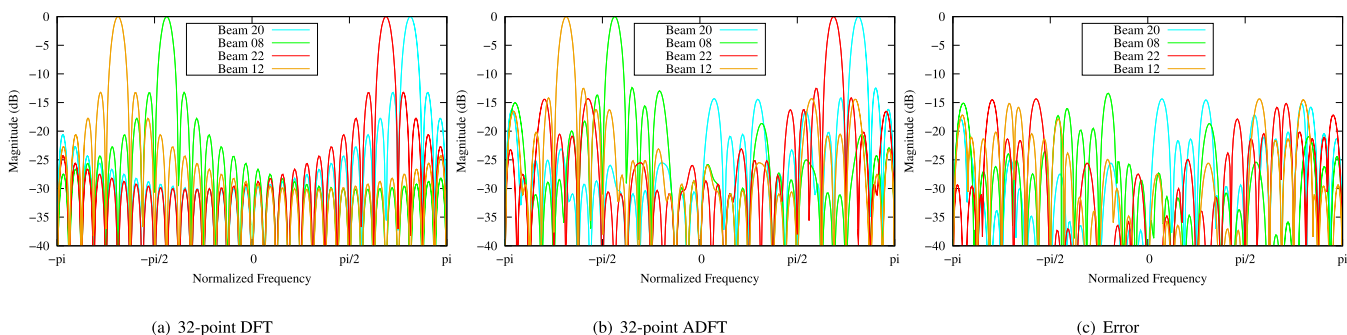


FIGURE 2. Magnitude of the filter-bank responses for (a) the exact 32-point DFT, (b) the 32-point ADFT and (c) error of the ADFT response for the least performing rows. .

**B. ARITHMETIC COMPLEXITY**

1) TWIDDLE-FACTOR MATRIX

In the three proposed algorithms, only the DFT computation  $F_{32}$  is subject to an approximation; the twiddle-factor matrix  $\Omega_{32}$  is left unaltered in its exact form (cf. (7)). Therefore, a minimum number of multiplications remains due to  $\Omega_{32}$ . Considering only the nontrivial multiplications, the twiddle-factor matrix requires 961 complex multiplications, which translate into 2883 real multiplications and 2883 real additions. The arithmetic complexity assumes sequential operation in a CPU. This parameter will be used in the arithmetic complexity calculations for each of the three algorithms.

2) ALGORITHM 1

Here the only source of multiplicative complexity are the twiddle factors in between the row- and column-wise 32-point ADFT blocks. Since the 32-point ADFT requires 348 additions and it is called 64 times, it contributes  $64 \times 348 = 22272$  real additions to the overall arithmetic complexity of Algorithm 1. The resulting arithmetic costs are: 2883 real multiplications and  $2883 + 22272 = 25155$  additions.

3) ALGORITHM 2

Here multiplicative costs stem from the twiddle factors and the column-wise 32-point exact DFT. The column-wise exact DFT is computed using the Cooley-Tukey radix-2 FFT [5], [38] (see Section III-B). Since this algorithm requires 32 calls to the exact 32-point DFT and 32 calls to the 32-point ADFT, we have a total of  $(32 \times 88) + 2883 = 5699$  real multiplications and  $(32 \times 408) + (32 \times 348) + 2883 = 27075$  real additions.

4) ALGORITHM 3

Here the operation count follows the same rationale as for Algorithm 2, with the difference that the roles of the row and column-wise transforms are swapped. Therefore, Algorithms 2 and 3 have the same arithmetic costs. The arithmetic complexity of the proposed methods is summarized in Table 1.

TABLE 1. Real arithmetic complexity for the exact 1024-point DFT and for the proposed approximations.

Algorithm	Real Mult.	Real Additions
Cooley-Tukey Radix-2 FFT [5, p. 76]	10,248	30,728
Split-Radix FFT [38]	7,172	27,652
Winograd FFT [41]	10,248	30,728
Proposed Algorithm 1	2,883	25,155
Proposed Algorithm 2	5,699	27,075
Proposed Algorithm 3	5,699	27,075

**C. PERFORMANCE OF THE PROPOSED APPROXIMATIONS**

Considering the frequency response error expressed in log-magnitude units, Fig. 3 shows (i) the upper and lower envelopes and (ii) the first, second, and third quartiles of the error resulting from the proposed approximate filter banks [47], [48]. For ease of visual inspection, we show only the normalized frequencies on the interval  $[-\pi/4, \pi/4]$ . The error of the frequency response for the remaining parts of the interval  $[-\pi, \pi]$  are just a repetition of the plots in Fig. 3.

Note that the three approximations resulting from Algorithm 1, Algorithm 2, and Algorithm 3 have distinct frequency responses. Fig. 3 indicates that the Algorithm 1 is the one presenting the largest deviation for the main lobe from the exact DFT. This is expected given that the transform resulting from Algorithm 1 is obtained through the substitution of both the row- and column-wise DFT block by the discussed approximate 32-point DFT. This qualitative analysis is confirmed once we calculate the errors in the frequency responses of the rows of the three proposed approximations. Table 2 displays the minimum (nonzero), mean, and maximum for the squared magnitude of these errors. Notice in Fig. 3 that the transform resulting from Algorithm 1 has the highest deviations from the expected frequency response for its rows with range of 5 dB compared to the filter bank response of the exact DFT matrix. In Table 2, we also show the worst-case side lobe in dB for each of the transforms. All transforms considered here possess a low worst-case side lobe on the order of  $-12$  dB.

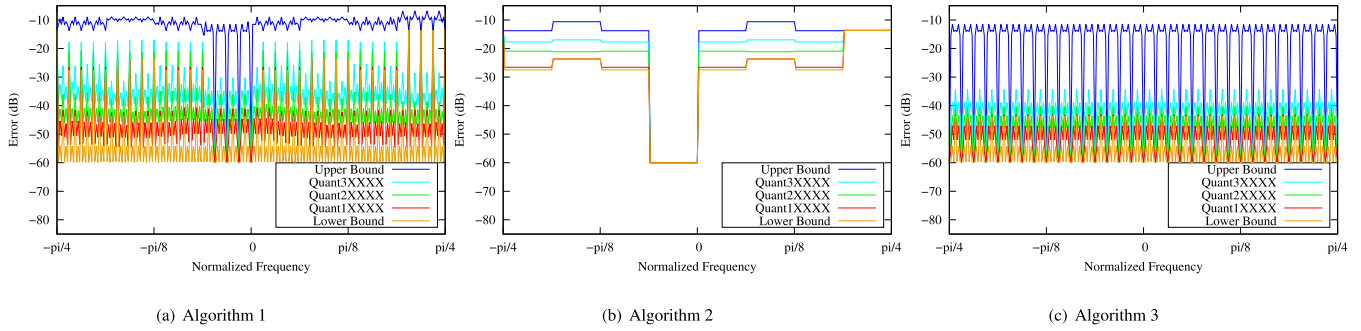


**FIGURE 3.** Log-magnitude error of the frequency response of the rows of the proposed approximations. The errors are bounded to  $-60$  dB for displaying purposes.

Noise rejection of the proposed ADFTs can be evaluated by means of its SNR improvement per frequency bin. The noise present from the antenna array can be modeled as additive white Gaussian noise (AWGN) with zero mean and variance  $\sigma^2$ . The AWGN present in each frequency bin is  $\sigma^2/N$ . For narrowband (monochromatic) plane wave received by the array, the input signals to both the DFT and the three ADFT algorithms follows  $\exp(j2\pi nk/N)$  for  $n, k = 0, 1, \dots, N-1$ , where  $k$  represents the DFT/ADFT bin number (corresponding to specific spatial frequencies related to the direction of propagation of each wave) and  $n$  is the antenna number in the ULA. The monochromatic signal having frequency  $\exp(j2\pi k/N)$  for bin  $k$  has its SNR improved by  $10 \log_{10}(N)$ , which is 30.1 dB for the 1024 point DFT. This is the best case SNR improvement per bin for the DFTs. The adoption of various ADFTs in place of the DFT causes a loss of SNR performance observed as a hit in the SNR per bin. Let the reduction in SNR for bin  $k$  be denoted  $\Delta\gamma_x$  where  $x \in \{1, 2, 3\}$  are for the three proposed approximation algorithms.

The worst-case SNR degradation for the ADFTs obtained through simulations with  $10^5$  replicates for finding the ensemble average for each bin of the ADFTs are shown in Table 2. The SNR degradation shows that Algorithm 1 has the largest worst-case degradation of SNR compared to the DFT ( $\Delta\gamma_1 < 0.9$  dB). There is no significant difference between Algorithm 2 and Algorithm 3 in terms of SNR degradation and has worst-case ( $\Delta\gamma_{2,3} < 0.4$  dB). The reduction in SNR of the three ADFTs compared to SNR of DFTs can be compensated by adding  $\leq 0.9$  dB of additional transmit power and antenna gain at the transmit side. Fig. 4 shows the SNR plot for each of the beams of the DFT and the three proposed approximations. Notice that no approximation has an SNR lower than 29.2 dB in any of the bins, demonstrating that the SNR degradation is  $\leq 0.9$  dB compared to the DFT where the SNR improves by 30.1 dB for every bin.

### V. DIGITAL VLSI REALIZATION

Next, we explore digital VLSI realizations of the three ADFT approaches outlined in (18), (19) and (19) using a time-multiplexed approach. Traditionally, arithmetic complexity amounts of counts of both multiplication operations and

addition operations. However, for semi-parallelized hardware implementations on VLSI platforms, the existence of parallel sub-systems offers a trade-off between circuit complexity and algorithm execution speed as described by Amdahl's Law [49]. The proposed algorithms are based on radix-32 SFGs, which imply the sequential nature is limited to 1024-point algorithm completion every 32 clock cycles. The radix-32 SFG allows re-use of ADFT and DFT cores, and twiddle-factor cores, using time-multiplexing up to 32 levels. The use of time-multiplexed operations leads to the generalization of the multiplier structures that do not distinguish trivial multiplications by 0, 1,  $-1$ . Therefore, the number of multiplications for the twiddle factor block is 1024 complex multiplications (compare to 961 complex multiplications for a sequential algorithm that can ignore trivial multiplications). However, radix-32 approach allows time-multiplexing of 32 parallel complex multipliers for achieving the twiddle factor matrix, leading to circuit complexity of 96 real multipliers, and 160 real adders/subtractors, in the twiddle factor block. To distinguish the mathematical operations from its physical realization, hereafter we refer to the circuit implementation of the selected 32-point DFT and ADFT, respectively, as DFT32 and ADFT32 cores. Also, the digital VLSI hardware for the 1024-point exact DFT and each of the 1024-point approximations resulting from Algorithm 1, Algorithm 2, and Algorithm 3 are referred to as the DFT1024, ADFT1024\_1, ADFT1024\_2, and ADFT1024\_3 cores, respectively. Fig. 5 shows the overall architecture of the DFT1024 with the DFT32 cores. We focus on the design of the ADFT1024\_1 core. Because this design can be easily extended to the other cores, the description of the ADFT1024\_2 (Algorithm 2) and ADFT1024\_3 (Algorithm 3) cores is omitted for brevity.

The core ADFT1024\_1 is a radix-32 unit and therefore processes an input signal block of 1024 time-domain samples in 32 clock cycles. Each signal block consists of 32 rows of adjacent time-domain samples in 32 columns. The first ADFT32 block sequentially computes the 32-point ADFT of each row, which are given by:  $x[k], x[32+k], x[2 \times 32 + k], \dots, x[31 \times 32 + k]$ , for  $k = 0, 1, \dots, 31$ . Sampled values in the intermediate frequency (IF) domain are



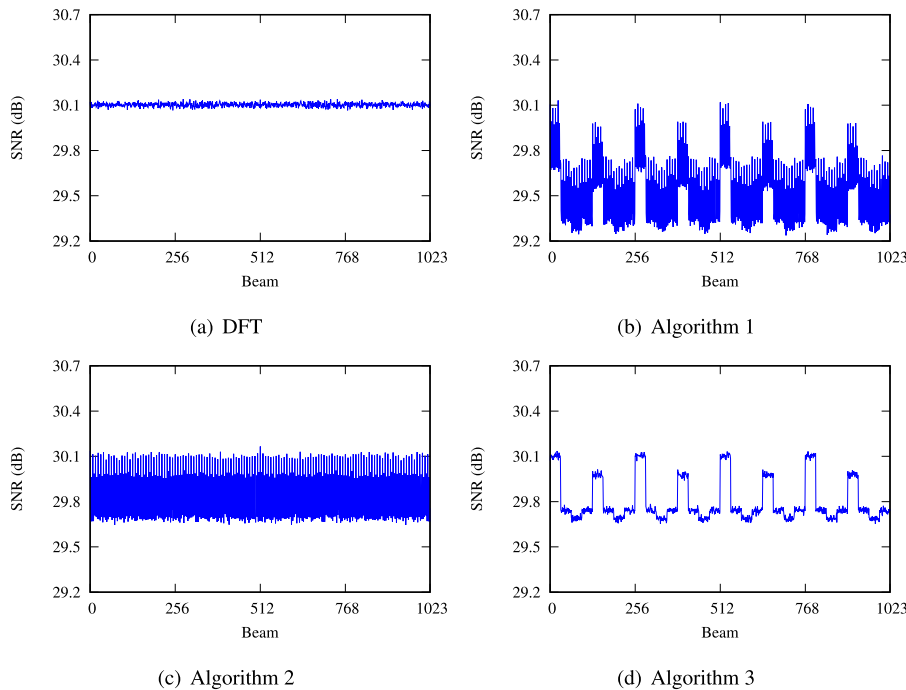


**FIGURE 4.** The SNR for DFT and proposed Algorithm 1, Algorithm 2, and Algorithm 3. The SNR for the proposed algorithms is no lower than 29.2 dB, against 30.1 dB for the DFT.

**TABLE 2.** Performance statistics of the proposed approximations: frequency response magnitude, worst-case side lobe level and SNR degradation.

Transform	Error Magnitude of Rows			Worst Side Lobe (dB)	SNR degradation (dB)
	Min (dB)	Mean (dB)	Max (dB)		
Algorithm 1	-10.7	-5.5	-4.4	-12.8	-0.6
Algorithm 2	-10.7	-9.9	-9.0	-12.8	-0.3
Algorithm 3	-10.7	-9.9	-9.0	-12.9	-0.3

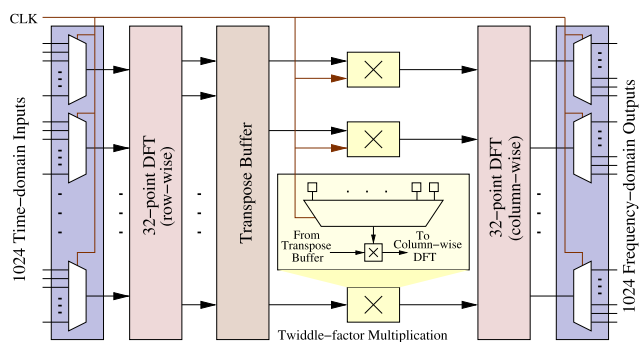


**FIGURE 5.** Signal flow graph showing the VLSI architecture to be modified for the proposed architecture based on the selected approximation. **Algorithm 1:** Replacement of both 32-point DFTs with 32-point ADFT blocks. **Algorithm 2:** Replacement of only row-wise 32-point DFT with 32-point ADFT blocks leaving column-wise DFT exact. **Algorithm 3:** Replacement of column-wise 32-point FFT with 32-point ADFT blocks leaving row-wise DFT exact.

passed to the transpose buffer, which realizes the matrix transposition operation in digital VLSI hardware, while operating in-step with the system clock. One complete matrix transpose operation is achieved every 32 clock cycles. The transpose buffer feeds the second time-multiplexed ADFT 32

after suitable twiddle factors have been applied, which in turn, furnishes the desired 1024-point ADFT values. In order to minimize the chances of overflow, the second time-multiplexed ADFT 32 block in Fig. 5 uses a larger wordlength by one bit than the first time-multiplexed ADFT 32 block. Use of a larger word length accommodates for the arithmetic operations that are carried on the first time-multiplexed ADFT 32 and the twiddle factors.

**A. TRANSPOSE BUFFER AND TWIDDLE FACTORS**

The transpose buffer shown in Fig. 6 consists of a mesh of 1024 delays and 32 parallel multiplexers, each of them possessing 32 inputs. The transpose buffer block generates the transpose of the first set of frequency bins. The transposition allows the column-wise DFT computation required in eq. (18), (19) and (20).

Twiddle-factor multiplication count consists of 961 non-trivial complex multiplications spread over 32 clock cycles. However, these are implemented using 32 parallel complex multipliers, which each consume 3 real multipliers and 5 adders (Gauss Algorithm for complex multiplication). The twiddle factor block therefore furnishes the only

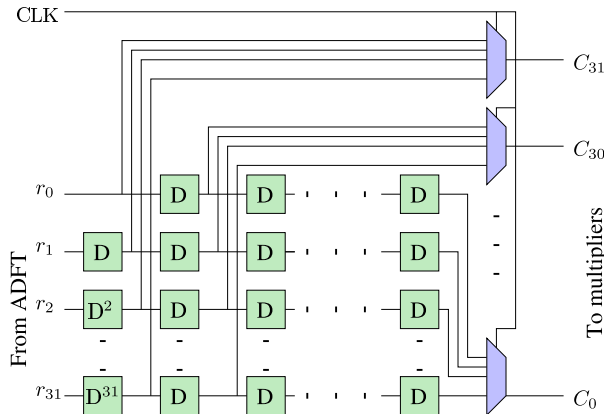


FIGURE 6. Schematic diagram of the transpose buffer.

multiplications present in ADFT1024\_1, which results from Algorithm 1 in a radix-32 hardware realization. Each of the column bins (after the transpose buffer) undergoes a multiplication by  $\omega_{1024}^{m \cdot n}$ , where  $0 \leq m \leq 31$  and  $0 \leq n \leq 31$ .

Therefore, the precision of the twiddle-factor multipliers plays a critical role in the final area  $A$ , area-time  $AT$ , and area-time-squared ( $AT^2$ ) metrics. In this paper, we have set the twiddle-factor precision level to be equal to the system word size of the inputs to the ADFT1024\_1 core, which is a design parameter and the choice of lower precision levels in the twiddle factors would result in improvements in the VLSI metrics for all three proposed algorithms. In a sense, hardware designed with such conservative parameters can be thought of as worst-case benchmark, with more coarsely quantified twiddle factors leading to even better improvements in area, area-time, and area-time-squared metrics.

### B. CIRCUIT COMPLEXITY

All circuits operate for 32 clock cycles to produce one 1024-point transform. Complex multiplication is realized using 3 real multiplier circuits and 5 real adder circuits following the Gauss multiplication algorithm. The twiddle-factor matrix based on Gauss multiplication  $\Omega_{32}$  in (18) therefore requires 96 real multiplier circuits and 160 adders circuits. This block is common to all four 1024-point algorithms.

#### 1) ADFT1024\_1 CORE

Each ADFT32 requires 348 adders/subtractors and no multipliers.

As shown in Fig. 5, the proposed radix-32 time-multiplexed architecture for Algorithm 1 uses two ADFT32 cores. Thus, ADFT1024\_1 has an overall circuit complexity of  $348 * 2 + 160 = 856$  adders/subtractor circuits and 96 real multiplier circuits.

#### 2) ADFT1024\_2 CORE

In ADFT1024\_2, the row-wise DFT block is substituted by the ADFT32 block. The DFT32 requires a total 78 real multiplier circuits and 398 adder circuits. Because the ADFT32 requires 348 adder circuits but no multipliers, we have an

TABLE 3. Circuit complexity for the proposed architectures and the 1024-point DFT.

Design	Multiplier Circuits	Adder Circuits
DFT1024	252	959
ADFT1024_1	96	856
ADFT1024_2	174	906
ADFT1024_3	174	906

overall circuit complexity of  $398 + 160 + 348 = 906$  adder circuits and  $96 + 78 = 174$  multipliers ADFT1024\_2.

#### 3) ADFT1024\_3 CORE

The circuit complexity for the Algorithm 3 is the same as for ADFT1024\_2. The only change is in the placement of the elements in the architectural level.

The 1024-point DFT (denoted DFT1024) obtained by using two DFT32 cores for row- and column-wise FFTs would require  $78 * 2 + 96 = 252$  real multiplier circuits and  $398 * 2 + 160 = 796 + 160 = 956$  adder circuits. This is our reference radix-32 FFT circuit for baselining the circuit complexities of the proposed ADFT1024 algorithms.

The circuit complexities for the proposed designs as well as DFT1024 are presented in Table 3.

### C. ASIC SYNTHESIS AND PLACE-ROUTE RESULTS: 45nm CMOS

The proposed architectures were implemented on MATLAB Simulink using Xilinx libraries and then mapped to 45-nm complementary metal-oxide semiconductor (CMOS) technology cells (synthesis only). Each of the designs consists of three main hardware components—first 32-point transform block, transpose buffer with twiddle-factor multiplication block, and second 32-point transform block. The complexity of each 32-point transform block core depends on its corresponding input word length. Key quantitative measurements of performance for each 32-point transform block core and transpose buffer with twiddle-factor multiplications are shown in Table 4. In Table 5, we list the hardware implementation metrics for ADFT1024\_1, ADFT1024\_2, and ADFT1024\_3. Metrics for the DFT1024 core were included as reference values.

### D. ANALYSIS OF THE RESULTS

The results in Table 4 shows that the 32-point ADFT core demands considerably less hardware resources than the 32-point exact DFT core. On the other hand, the implementation of the transpose buffer with twiddle factor multiplication adds a fixed hardware complexity to the system for both the DFT and the approximate architectures. As a result, the transpose buffer causes the highest area consumption and a relatively high power consumption in comparison to that of 32-point ADFT cores. Thus, it becomes the dominant

**TABLE 4.** Key quantitative measurements of performance in digital 45 nm CMOS VLSI for each DFT core and transpose buffer with twiddle factor multiplications.

Performance Metric	Row-wise transform			Transpose buffer with multipliers	Column-wise transform		
	DFT32	ADFT32	Change		DFT32	ADFT32	Change
Area, $A$ (mm <sup>2</sup> )	4.43	1.02	76.94 % ↓	6.90	6.83	1.47	78.43 % ↓
Critical Path Delay, $T$ (ns)	1.88	1.82	3.14 % ↓	1.82	1.88	1.82	3.14 % ↓
Frequency, $F_{max}$ (GHz)	0.53	0.55	3.24 % ↑	0.55	0.53	0.55	3.24 % ↑
$AT$ (mm <sup>2</sup> ns)	8.33	1.86	77.67 % ↓	12.56	12.85	2.69	79.10 % ↓
$AT^2$ (mm <sup>2</sup> ns <sup>2</sup> )	15.68	3.39	78.37 % ↓	22.86	24.18	4.90	79.76 % ↓
Dynamic Power, $D_p$ (mW/GHz)	10.08	2.00	80.13 % ↓	10.44	24.29	2.79	88.5 % ↓

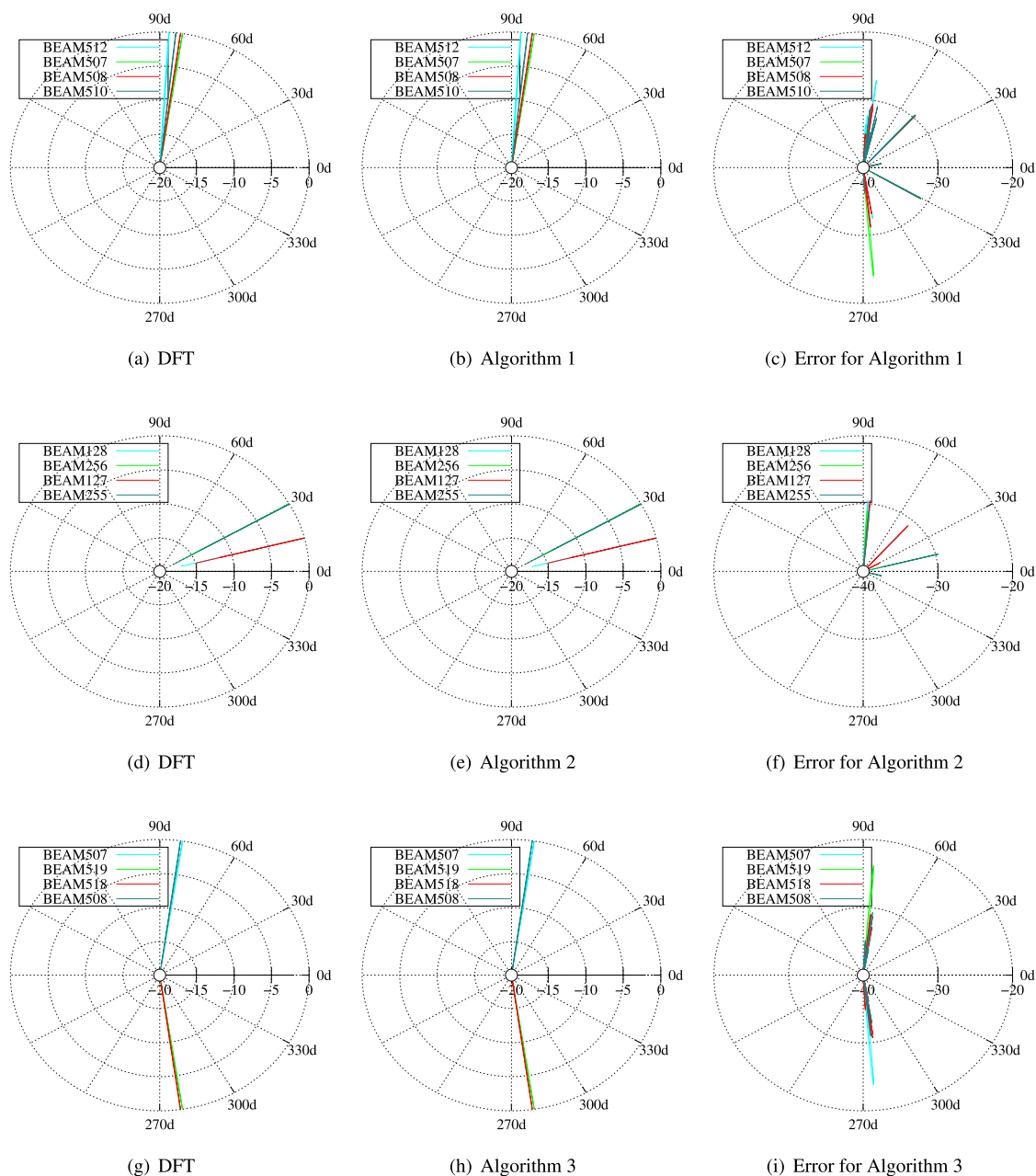


**FIGURE 7.** The four worst bins for multi-beam beamforming: (a) exact DFT response, (b) ADFT response, and (c) error for algorithm 1; (d) exact DFT response, (e) ADFT response, and (f) error for algorithm 2; (g) exact DFT response, (h) ADFT response, and (i) error for algorithm 3.

TABLE 5. Key quantitative measurements of performance in digital 45 nm CMOS VLSI for each algorithm.

Performance Metric	DFT1024	ADFT1024_1		ADFT1024_2		ADFT1024_3	
		Value	Change	Value	Change	Value	Change
Area, $A$ ( $\text{mm}^2$ )	18.16	9.40	48.25% ↓	14.75	18.76% ↓	12.80	29.49% ↓
Critical Path Delay, $T$ (ns)	1.88	1.82	3.14% ↓	1.88	-	1.88	-
Frequency, $F_{\text{max}}$ (GHz)	0.53	0.55	3.20% ↑	0.53	-	0.53	-
$AT$ ( $\text{mm}^2\text{ns}$ )	34.17	17.13	49.89% ↓	27.76	18.76% ↓	24.10	29.49% ↓
$AT^2$ ( $\text{mm}^2\text{ns}^2$ )	64.31	31.23	51.45% ↓	52.25	18.76% ↓	45.35	29.49% ↓
Dynamic Power, $D_p$ (mW/GHz)	44.81	15.24	66.00% ↓	36.73	18.02% ↓	23.31	47.98% ↓

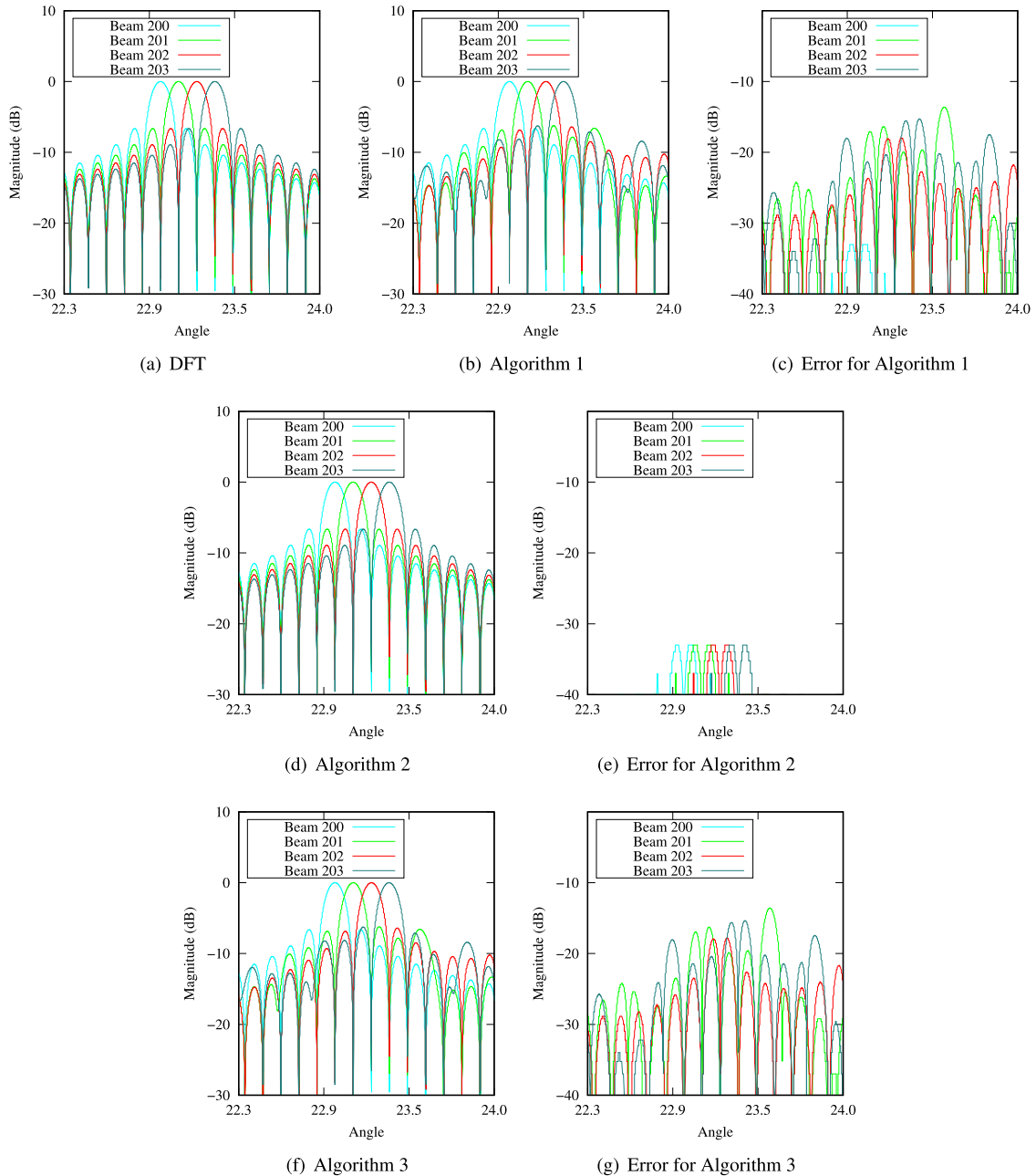


FIGURE 8. Linear plot of selected beams {200, 201, 202, 203} for exact and approximate transforms: (a) exact DFT response, (b) ADFT response, and (c) error for algorithm 1; (d) ADFT response, and (e) error for algorithm 2; (f) ADFT response, and (g) error for algorithm 3.

factor in hardware complexity for the designs of the three 1024-point approximate transforms, as shown in Table 5.

The core ADFT1024\_1 gives the best hardware utilization, whereas ADFT1024\_2 gives the worst as can be seen in Table 5. Algorithm 3 gives the best error performance, i.e., provides the most accurate approximation. Moreover, the hardware resource consumption of its physical realization ADFT1024\_3 is also close to that of ADFT1024\_2. The error performance of Algorithm 2 does not differ much from that of Algorithm 1, which also provides a hardware realization ADFT1024\_1 with the lowest resource consumption. Therefore, we recommend either Algorithm 1 or Algorithm 3 (i.e., its hardware realizations ADFT1024\_1 and ADFT1024\_3) as the best designs.

### E. ADFT-BASED 1024-BEAM DIGITAL BEAMFORMERS

In the proposed system, each ADFT bin corresponds to a unique direction in space. Ideally these bins should be identical to the spatial DFT bins, but their magnitude could deviate because of the approximation. The four worst bins for each of the three algorithms are shown in Fig. 7. The resulting errors are small enough to be acceptable for the low SNR scenarios seen in practical wireless systems.

Fig. 8 shows detailed plots of 4 consecutive beams (from bins 200-203) for the three proposed algorithms, together with the errors. We chose these four beams arbitrarily to showcase the shapes of the obtained RF beams in sufficient detail.

Note that practical realization of 1024-element ULAs for generating narrow ADFT-based beams in currently-licensed frequency bands (upto the V band) may be challenging due to the large sizes of the resulting apertures. However, due to ongoing research in the sub-THz range [24]–[32], the W and G bands will soon be commercially available for both licensed and unlicensed use. At a carrier frequency of 300 GHz,  $\lambda/2 = 0.5$  mm and thus the size of a Nyquist-spaced 1024-element ULA would decrease to a reasonable value of 51.2 cm.

### VI. CONCLUSIONS

FFTs are used for reducing the computational costs of evaluating the DFT. Generally, they decrease complexity from  $\mathcal{O}(N^2)$  down to  $\mathcal{O}(N \log N)$ . In this paper, we show that further savings can be accomplished by means of approximate methods. The resulting 1024-point DFT approximations present a trade-off between performance and hardware complexity without significant loss in terms of worst-side lobe and SNR.

Our work shows that larger block-length DFT approximations can be obtained from the smaller-size approximations derived using previously-described numerical optimization methods. Our methodology can be directly applied to any DFT for which the block length is a perfect square. Since the current DFT approximations in the literature are restricted to the sizes {8, 16, 32} [8], [35], [48], [50], [51], approximate algorithms can be derived for  $N \in \{64, 256, 1024\}$ . In this

work, we focused on the 1024-point case. Assuming that a multiplierless DFT approximation of size  $\sqrt{N}$  can always be found, our derivations suggests that we can obtain an  $N$ -point DFT approximation that requires only  $N - 2\sqrt{N} - 1$  multiplications; effectively making the complexity of the resulting  $N$ -point approximation  $\mathcal{O}(N)$ . The proposed algorithms were synthesized to digital VLSI using a 45-nm CMOS library. Synthesis results confirm the expected improvements in layout area and power consumption metrics compared to a conventional 1024-point DFT implementation.

The choice of algorithm depends on the application and its tolerance for computational error in the DFT block. Highly error tolerant applications can greatly benefit from Algorithm 1 which has the lowest complexity. Algorithm 2 or 3 maybe selected when Algorithm 1 does not furnish sufficient performance.

### REFERENCES

- [1] Z. Zhang, X. Wang, K. Long, A. V. Vasilakos, and L. Hanzo, "Large-scale MIMO-based wireless backhaul in 5G networks," *IEEE Wireless Commun.*, vol. 22, no. 5, pp. 58–66, Oct. 2015.
- [2] S. Sun, T. Rappaport, R. Heath, A. Nix, and S. Rangan, "MIMO for millimeter-wave wireless communications: Beamforming, spatial multiplexing, or both?" *IEEE Commun. Mag.*, vol. 52, no. 12, pp. 110–121, Dec. 2014.
- [3] A. Adhikary, J. Nam, J.-Y. Ahn, and G. Caire, "Joint spatial division and multiplexing—The large-scale array regime," *IEEE Trans. Inf. Theory*, vol. 59, no. 10, pp. 6441–6463, Oct. 2013.
- [4] D. C. Champeney, *A Handbook of Fourier Theorems*. Cambridge, U.K.: Cambridge Univ. Press, 1987.
- [5] R. E. Blahut, *Fast Algorithms for Signal Processing*. Cambridge, U.K.: Cambridge Univ. Press, 2010.
- [6] A. V. Oppenheim and R. W. Schaffer, *Discrete-Time Signal Processing*, 3rd ed. Upper Saddle River, NJ, USA: Prentice-Hall, 2009.
- [7] A. Madanayake, S. Mandal, T. S. Rappaport, V. Ariyaratna, S. Madishetty, S. Pulipati, R. J. Cintra, D. Coelho, R. Oliviera, F. M. Bayer, and L. Belostotski, "Towards a low-SWaP 1024-beam digital array: A 32-beam subsystem at 5.8 GHz," *IEEE Trans. Antennas Propag.*, vol. 68, no. 2, pp. 900–912, Feb. 2020.
- [8] V. Ariyaratna, D. F. G. Coelho, S. Pulipati, R. J. Cintra, F. M. Bayer, V. S. Dimitrov, and A. Madanayake, "Multibeam digital array receiver using a 16-point multiplierless DFT approximation," *IEEE Trans. Antennas Propag.*, vol. 67, no. 2, pp. 925–933, Feb. 2019.
- [9] S. W. Ellingson and W. Cazemier, "Efficient multibeam synthesis with interference nulling for large arrays," *IEEE Trans. Antennas Propag.*, vol. 51, no. 3, pp. 503–511, Mar. 2003.
- [10] J. O. Coleman, "A generalized FFT for many simultaneous receive beams," Naval Res. Lab, Signal Process. Sect., Washington, DC, USA, Tech. Rep. NRL/MR/5320-07-9029, 2007.
- [11] C. Y. C. Yang, Y.-Z.-X. Y.-Z. Xie, L. C. L. Chen, H. C. H. Chen, and Y. D. Y. Deng, "Design of a configurable fixed-point FFT processor," in *Proc. IET Int. Radar Conf.*, Oct. 2015, pp. 1–4.
- [12] C. V. Kumar and K. R. K. Sastry, "Design and implementation of FFT pruning algorithm on FPGA," in *Proc. 7th Int. Conf. Cloud Comput., Data Sci. Eng.-Confluence*, Jan. 2017, pp. 739–743.
- [13] T. Ayhan, W. Dehaene, and M. Verhelst, "A 128:2048/1536 point FFT hardware implementation with output pruning," in *Proc. 22nd Eur. Signal Process. Conf. (EUSIPCO)*, Sep. 2014, pp. 266–270.
- [14] M. Z. A. Khan and S. Qadeer, "A new variant of Radix-4 FFT," in *Proc. 13th Int. Conf. Wireless Opt. Commun. Netw. (WOCN)*, Jul. 2016, pp. 1–4.
- [15] M. T. Heideman, "Multiplicative complexity of linear and bilinear systems," in *Multiplicative Complexity, Convolution, and the DFT*. New York, NY, USA: Springer, 1988, pp. 5–26.
- [16] V. Ariyaratna, A. Madanayake, X. Tang, D. Coelho, R. J. Cintra, L. Belostotski, S. Mandal, and T. S. Rappaport, "Analog approximate-FFT 8/16-beam algorithms, architectures and CMOS circuits for 5G beamforming MIMO transceivers," *IEEE J. Emerg. Sel. Topics Circuits Syst.*, vol. 8, no. 3, pp. 466–479, Sep. 2018.



- [17] T. S. Rappaport, S. Sun, R. Mayzus, H. Zhao, Y. Azar, K. Wang, G. N. Wong, J. K. Schulz, M. Samimi, and F. Gutierrez, "Millimeter wave mobile communications for 5G cellular: It will work!," *IEEE Access*, vol. 1, pp. 335–349, 2013.
- [18] T. S. Rappaport, Y. Xing, O. Kanhere, S. Ju, A. Madanayake, S. Mandal, A. Alkhatieb, and G. C. Trichopoulos, "Wireless communications and applications above 100 GHz: Opportunities and challenges for 6 G and beyond," *IEEE Access*, vol. 7, pp. 78729–78757, 2019.
- [19] E. Bjornson, L. Sanguinetti, H. Wymeersch, J. Hoydis, and T. L. Marzetta, "Massive MIMO is a reality—What is next?: Five promising research directions for antenna arrays," *Digital Signal Process.*, vol. 94, pp. 3–20, Nov. 2019.
- [20] H. Wymeersch, G. Seco-Granados, G. Destino, D. Dardari, and F. Tufvesson, "5G mmWave positioning for vehicular networks," *IEEE Wireless Commun.*, vol. 24, no. 6, pp. 80–86, Dec. 2017.
- [21] E. Marchand, H. Uchiyama, and F. Spindler, "Pose estimation for augmented reality: A hands-on survey," *IEEE Trans. Vis. Comput. Graphics*, vol. 22, no. 12, pp. 2633–2651, Dec. 2016.
- [22] A. Taha, M. Alrabeiah, and A. Alkhatieb, "Enabling large intelligent surfaces with compressive sensing and deep learning," 2019, *arXiv:1904.10136*. [Online]. Available: <https://arxiv.org/abs/1904.10136>
- [23] IEEE Communication Society. *Technology Blog*. Accessed: Oct. 16, 2019. [Online]. Available: <https://techblog.comsoc.org/category/5g/>
- [24] M. Hossain, K. Nosaeva, B. Janke, N. Weimann, V. Krozer, and W. Heinrich, "A G-band high power frequency doubler in transferred-substrate InP HBT technology," *IEEE Microw. Wireless Compon. Lett.*, vol. 26, no. 1, pp. 49–51, Jan. 2016.
- [25] K. Zhou, J.-Q. Ding, C.-X. Zhou, and W. Wu, "W-Band dual-band quasi-elliptical waveguide filter with flexibly allocated frequency and bandwidth ratios," *IEEE Microw. Wireless Compon. Lett.*, vol. 28, no. 3, pp. 206–208, Mar. 2018.
- [26] A. Kurdoghlian, H. Moyer, H. Sharifi, D. F. Brown, R. Nagele, J. Tai, R. Bowen, M. Wetzel, R. Grabar, D. Santos, and M. Micovic, "First demonstration of broadband W-band and D-band GaN MMICs for next generation communication systems," in *IEEE MTT-S Int. Microw. Symp. Dig.*, Jun. 2017, pp. 1126–1128.
- [27] W. Shaobing, G. Jianfeng, W. Weibo, and Z. Junyun, "W-band MMIC PA with ultrahigh power density in 100-nm AlGaIn/GaN technology," *IEEE Trans. Electron Devices*, vol. 63, no. 10, pp. 3882–3886, Oct. 2016.
- [28] S. Carpenter, Z. S. He, and H. Zirath, "Balanced active frequency multipliers in d and g bands using 250nm InP DHB technology," in *Proc. IEEE Compound Semiconductor Integr. Circuit Symp. (CSICS)*, Oct. 2017, pp. 1–4.
- [29] M. Rodwell, Z. Griffith, N. Parthasarathy, E. Lind, C. Sheldon, S. Bank, U. Singiseti, M. Urteaga, K. Shinohara, R. Pierson, and P. Rowell, "Developing bipolar transistors for sub-mm-wave amplifiers and next-generation (300 GHz) digital circuits," in *Proc. 64th Device Res. Conf.*, Jun. 2006, pp. 5–8.
- [30] J. Kim and J. F. Buckwalter, "Staggered gain for 100+ GHz broadband amplifiers," *IEEE J. Solid-State Circuits*, vol. 46, no. 5, pp. 1123–1136, May 2011.
- [31] A. Natarajan, A. Komijani, X. Guan, A. Babakhani, and A. Hajimiri, "A 77-GHz phased-array transceiver with on-chip antennas in silicon: Transmitter and local LO-path phase shifting," *IEEE J. Solid-State Circuits*, vol. 41, no. 12, pp. 2807–2819, Dec. 2006.
- [32] A. Babakhani, X. Guan, A. Komijani, A. Natarajan, and A. Hajimiri, "A 77-GHz phased-array transceiver with on-chip antennas in silicon: Receiver and antennas," *IEEE J. Solid-State Circuits*, vol. 41, no. 12, pp. 2795–2806, Dec. 2006.
- [33] Y. Xing and T. S. Rappaport, "Propagation measurement system and approach at 140 GHz—moving to 6G and above 100 GHz," in *Proc. IEEE Global Commun. Conf. (GLOBECOM)*, Dec. 2018, pp. 1–6.
- [34] Y. Xing, O. Kanhere, S. Ju, and T. S. Rappaport, "Indoor wireless channel properties at millimeter wave and sub-terahertz frequencies," in *Proc. IEEE Global Commun. Conf. (GLOBECOM)*, Dec. 2019, pp. 1–6.
- [35] D. M. S. Villagrán, "Aproximações para a transformada discreta de Fourier e aplicações em detecção e estimação," M.S. thesis, Dept. Statist., Univ. Federal de Pernambuco, Recife, Brazil, 2015.
- [36] K. R. Rao and P. C. Yip, Eds., *The Transform and Data Compression Handbook* (Electrical Engineering & Applied Signal Processing Series). Boca Raton, FL, USA: CRC Press, 2000.
- [37] J. W. Cooley and J. W. Tukey, "An algorithm for the machine calculation of complex Fourier series," *Math. Comput.*, vol. 19, no. 90, pp. 297–301, 1965.
- [38] P. Duhamel and H. Hollmann, "Split radix FFT algorithm," *Electron. Lett.*, vol. 20, no. 1, pp. 14–16, 1984.
- [39] S. Winograd, "On computing the discrete Fourier transform," *Math. Comput.*, vol. 32, no. 141, pp. 175–199, 1978.
- [40] S. Winograd, "On the multiplicative complexity of the discrete Fourier transform," *Adv. Math.*, vol. 32, no. 2, pp. 83–117, May 1979.
- [41] S. Winograd, *Arithmetic Complexity of Computations* (CBMS-NSF Regional Conference Series in Applied Mathematics). Philadelphia, PA, USA: SIAM, 1980.
- [42] S. G. Johnson and M. Frigo, "A modified split-radix FFT with fewer arithmetic operations," *IEEE Trans. Signal Process.*, vol. 55, no. 1, pp. 111–119, Jan. 2007.
- [43] T. Duong. (2019). *Vec, Vech, Invvec, Invvech*. [Online]. Available: <https://www.rdocumentation.org/packages/ks/versions/1.6.13/topics/vec%20C%20vech%20invvec%20invvech>
- [44] MathWorks. (2019). *MATLAB R2018b Documentation 'Vec2mat'*. [Online]. Available: <https://www.mathworks.com/help/comm/ref/vec2mat>
- [45] MathWorks. (2019). *MATLAB R2018b Documentation 'Reshape'*. [Online]. Available: <https://www.mathworks.com/help/matlab/ref/reshape>
- [46] G. A. F. Seber, *A Matrix Handbook for Statisticians* (Wiley Series in Probability and Statistics). Hoboken, NJ, USA: Wiley, 2008.
- [47] D. Suarez, A. Sengupta, F. M. Bayer, A. Madanayake, S. Kulasekera, and R. J. Cintra, "Multi-beam RF aperture using multiplierless FFT approximation," *Electron. Lett.*, vol. 50, no. 24, pp. 1788–1790, Nov. 2014.
- [48] S. Kulasekera, A. Madanayake, R. J. Cintra, D. Suarez, and F. M. Bayer, "Multi-beam receiver apertures using multiplierless 8-point approximate DFT," in *Proc. IEEE Radar Conf. (RadarCon)*, May 2015, pp. 1244–1249.
- [49] G. M. Amdahl, "Validity of the single processor approach to achieving large scale computing capabilities," in *Proc. Spring Joint Comput. Conf.-AFIPS (Spring)*. New York, NY, USA: ACM, 1967, pp. 483–485.
- [50] V. A. Coutinho, V. Ariyaratna, D. F. G. Coelho, R. J. Cintra, and A. Madanayake, "An 8-beam 2.4 GHz digital array receiver based on a fast multiplierless spatial DFT approximation," in *IEEE MTT-S Int. Microw. Symp. Dig.*, Jun. 2018, pp. 1538–1541.
- [51] V. Ariyaratna, S. Kulasekera, A. Madanayake, K.-S. Lee, D. Suarez, R. J. Cintra, F. M. Bayer, and L. Belostotski, "Multi-beam 4 GHz microwave apertures using current-mode DFT approximation on 65 nm CMOS," in *IEEE MTT-S Int. Microw. Symp. Dig.*, May 2015, pp. 1–4.



**ARJUNA MADANAYAKE** (Member, IEEE) received the Ph.D. degree in electrical engineering from the University of Calgary, Alberta, Canada, in 2008. He is currently an Associate Professor of electrical and computer engineering with Florida International University (FIU) in Miami, FL. His research interests are in array signal processing, multi-dimensional systems and signal processing, microwave and analog circuits, digital circuits and FPGA systems, fast algorithms and applications, wireless communications, and mm-wave systems. His research program at FIU is funded by several grants from DARPA and NSF.



**RENATO J. CINTRA** (Senior Member, IEEE) received the D.Sc. degree in electrical engineering from the Universidade Federal de Pernambuco (UFPE), Brazil, in 2005. He joined the Centre for Natural and Exact Sciences, UFPE, in 2005. He has held visiting professor positions at the Département Informatique, INSA, Lyon, France and the University of Calgary, Canada. He was an Associate Editor for the IEEE GEOSCIENCE AND REMOTE SENSING LETTERS, and *Circuits, Systems, and Signal Processing* (Springer). He serves as an Associate Editor for *IET Circuits, Devices & Systems* and the *Journal of Communication and Information Systems*, and a Subject Editor of *ELECTRONICS LETTERS*. His long-term topics of research include: approximation theory for discrete transforms, theory and methods for digital signal/image processing, and statistical methods.



**NAJATH AKRAM** (Student Member, IEEE) received the B.Sc. degree in electrical and information engineering from the University of Ruhuna, Sri Lanka, in 2016. He is currently pursuing the Ph.D. degree with Florida International University under the supervision of Dr. Arjuna Madanayake. His research interests include multi-dimensional signal processing, RF systems design, and antenna array processing.



**FÁBIO M. BAYER** received the B.Sc. degree in mathematics from the Federal University of Santa Maria (UFSM), Brazil, in 2006, and the D.Sc. degree in statistics from the Federal University of Pernambuco (UFPE), Brazil, in 2011. He is currently an Associate Professor with the Department of Statistics, UFSM and a Researcher with the Laboratory of Space Sciences of Santa Maria (LACESM), UFSM. His research interests include data science, regression and dynamic models, statistical computing, parametric inference, and statistical signal processing.



**VIDUNETH ARIYARATHNA** (Student Member, IEEE) received the bachelor's degree (Hons.) in electronics and telecommunication engineering from the University of Moratuwa, Sri Lanka, in 2013, the master's degree in electrical engineering from the University of Akron, in 2016, under the supervision of Dr. Arjuna Madanayake, and the Ph.D. degree from Florida International University, in 2019, under the supervision of Dr. Arjuna Madanayake. He is currently a Postdoctoral Research Associate with the Ultra-Broadband Nanonetworking Laboratory, Northeastern University. His main research interests include the areas of RF-systems design, analog-digital hybrid beamforming systems, ultra-broadband wireless communication systems, and multi-dimensional signal processing.



**DIEGO COELHO** received the B.Sc. degree in electronics engineering and the M.Sc. degree in statistics from the Universidade Federal de Pernambuco (UFPE), Recife, Brazil, in 2012 and 2015, respectively, and the Ph.D. degree from the University of Calgary, Calgary, Canada, in 2018.

He is currently an Independent Researcher, Calgary, Canada. His research interests include digital signal and image processing, optimization, matrix computation, numerical analysis, and high-performance computing.

Assistant Professor with the Department of Electrical, Computer, and Systems Engineering, Case Western Reserve University, Cleveland, OH, USA. His research interests include the areas of RF-systems design, analog-digital hybrid beamforming systems, ultra-broadband wireless communication systems, and multi-dimensional signal processing.



**SOUMYAJIT MANDAL** (Senior Member, IEEE) received the B.Tech. degree in electronics and electrical communications engineering from IIT Kharagpur, India, in 2002, and the M.S. and Ph.D. degrees in electrical engineering from the Massachusetts Institute of Technology (MIT), Cambridge, MA, USA, in 2004 and 2009, respectively. He was a Research Scientist at Schlumberger-Doll Research, Cambridge, MA, USA, from 2010 to 2014. He is currently the T. and A. Schroeder



**THEODORE S. RAPPAPORT** (Fellow, IEEE) is currently the David Lee/Ernst Weber Professor with New York University (NYU) and holds faculty appointments with the Electrical and Computer Engineering Department of the NYU Tandon School of Engineering, the Courant Computer Science Department, and the NYU Langone School of Medicine. He is also the Founder and the Director of NYU WIRELESS, a multidisciplinary research center focused on the future of wireless communications and applications. His research has led the way for modern wireless communication systems. In 1987, his Ph.D. at Purdue University provided fundamental knowledge of indoor wireless channels used to create the first WiFi standard (IEEE 802.11), and he conducted fundamental work that led to the first US Digital cellphone standards, TDMA IS-54/IS-136, and CDMA IS-95. He and his students engineered the world's first public WiFi hotspots, and more recently, his work proved the viability of millimeter waves for mobile communications, and the global wireless industry adopted his vision for 5th generation (5G) cellphone networks. He founded three academic wireless research centers at Virginia Tech, The University of Texas, and NYU that have produced thousands of engineers and educators, since 1990, and he has coauthored over 300 articles and 20 books, including the most cited books on wireless communications, adaptive antennas, wireless simulation, and millimeter-wave communications. He co-founded two wireless companies, TSR Technologies and Wireless Valley Communication, which were sold to publicly traded companies, and he has advised many others. He co-founded the Virginia Tech Symposium on Wireless Communications, in 1991, the Texas Wireless Summit, in 2003, and the Brooklyn 5G Summit (B5GS), in 2014. He has more than 100 patents, serves on the Technological Advisory Council of the Federal Communications Commission (FCC)

Assistant Professor with the Department of Electrical, Computer, and Systems Engineering, Case Western Reserve University, Cleveland, OH, USA. His research interests include analog and biological computation, magnetic resonance sensors, low-power analog and RF circuits, and precision instrumentation for various biomedical and sensor interface applications. He was a recipient of the President of India Gold Medal, in 2002, the MIT Microsystems Technology Laboratories (MTL) Doctoral Dissertation Award, in 2009, the T. Keith Glennan Fellowship, in 2016, and the IIT Kharagpur Young Alumni Achievers Award, in 2018. He has over 125 publications in peer-reviewed journals and premier conferences, and has been awarded 18 patents.

Dr. Rappaport is a Fellow of the Radio Club of America and the National Academy of Inventors, a Life Member of the American Radio Relay League, a Licensed Professional Engineer in Texas and Virginia, and an Amateur Radio Operator (N9NB). He has received ASEE's Terman Award, the Sir Monty Finiston Medal from the Institution of Engineering and Technology (IET), the IEEE Vehicular Technology Society's James R. Evans Avant Garde and Stu Meyer Awards, the IEEE Education Society William E. Sayle Award for achievement in education, the IEEE Communications Society Armstrong Award, and the Armstrong Medal from the Radio Club of America.



**VÍTOR A. COUTINHO** received the B.Sc. degree in electronic engineering, the M.Sc. and D.Sc. degrees in electrical engineering from the Universidade Federal de Pernambuco, Recife, Brazil, in 2012, 2015, and 2018, respectively.

He is currently a Postdoctoral Researcher with the Universidade Federal de Pernambuco. His main research interests include digital signal processing, fast algorithms for discrete transforms, discrete transform approximations, and pruned-based algorithms for image compression.

...